Characterization of the channeling process in the scattering of relativistic electrons with periodic structures

Julio San Roman, Luis Plaja, Luis Roso, and Uwe Schwengelbeck
Departamento de Física Aplicada, Universidad de Salamanca, E-37008 Salamanca, Spain
(Received 20 December 2001; published 6 May 2002)

Most of the theoretical work about channeling of fast particles in crystal structures takes as a starting point a particle already in the target's bulk. In this paper, we address theoretically the channeling process itself, i.e., the injection of a relativistic electron from vacuum into the crystalline target. We show that, contrary to that general assumption, the target surface induces *longitudinal* as well as transversal dynamics into the channeled electron wave function. We present an efficient method for computing the eigenstates of the general relativistic electron-target scattering problem, and use it to the case of planar (110) channeling in silicon. The angular distribution of the transmitted electron is analyzed, and shown to depend strongly on the target thickness. In addition, we derive analytical closed formulas for the probability of the incident electron to be channeled in the different crystal states, and check their validity by comparison with the results of the exact numerical solutions. Finally, we identify the electron initial conditions that create a population inversion in the channeled states.

DOI: 10.1103/PhysRevA.65.052904 PACS number(s): 61.85.+p, 03.65.−w

I. INTRODUCTION

Channeling of relativistic particles along crystal symmetry axes or planes has been a constant subject of study for the last decades. Although first proposed by Stark in the 1920s [1], the feasibility of this process was confirmed in the early 1960s by the numerical computation of the transmission of fast ions through different targets [2]. These calculations gave the basis for interpreting the anomalous increase of the transmission of relativistic ions found in experiments when they were injected almost parallel to the direction of a crystal symmetry [3]. Channeled particles have exceptional characteristics: on one hand, they propagate almost ballistically inside the target, therefore with low dissipation; on the other hand, the strength of interaction of the particle with the crystal potential is effectively increased by the Lorentz boost. As a consequence, the channeled particles are good candidates for the experimental study of matter under high-static fields, in which intense field quantum effects, like pair creation, photon-photon collisions, etc., may be studied [4].

One of the most particular features of particle channeling is the anomalous increase of coherent brehmsstrahlung emission [5]. In comparison with the nonrelativistic case (see, for instance [6]), the relevant aspect of the channeling radiation consist in that the photon emitted are Doppler shifted to high energies (about 100 keV for an electron accelerated to a few tens of MeV), and therefore constitutes a promising source of hard x rays [7].

The theoretical grounds of the channeling process are, nowadays, well established. The energy spectrum of the channeled radiation can be successfully recovered by model potentials [8,9]. However, to the authors' knowledge, little effort has been directed to the study of the quantitative description of the channeling process, since the general starting point is a particle already propagating in the crystal bulk. The spontaneous character of the channeling radiation relates its intensity with the amount of population in the excited channeled states. Obviously, these are greatly dependent on the particle's wave function before entering the target, and on the nature of the scattering with the target-vacuum interface. In this context, the study of the channeling process of, initially, a free particle is well justified. In addition, the proper addressing of this problem allows one to delimit under what circumstances a population inversion in the channel states can be achieved, which is a relevant aspect for any possible future scheme of coherent amplification. The aim of this paper is to address these questions by solving the eigenstate problem of the free — propagating in vacuum — particle injected into the target potential.

The following section contains the statement of the general problem of the scattering of a relativistic particle with a target potential. A slow-envelope assumption is used to derive the equations for the eigenstates of this problem. Section III shows how these eigenstates can be computed efficiently in an exact manner, without the need to diagonalize the three-dimensional Hamiltonian. In particular, the case of a particle injected in almost parallel to the (110) plane of Si is addressed. We devote Sec. IV to the computation of the distribution of probabilities of the incident particle over the different channeled states. We derive analytical closed-form expressions for these probabilities assuming an approximated tight-binding model. The accuracy of these formulas is checked by comparison to the exact numerical solution. Finally, under the light of this model, we discuss the possibility of obtaining population inversion in the channeled states.

II. SCATTERING OF A RELATIVISTIC PARTICLE INTO THE TARGET

Consider the general problem of a relativistic electron, traveling initially in vacuum with a trajectory almost parallel to the x axis, injected into a space-limited target. Let us assume that the target potential is free of singularities and, therefore, it encloses only low —- nonrelativistic — momentum components (a valid approximation in the vast majority of targets). In this case, the trajectory of the scattered particle will be still dominated by the initial momentum, and there-

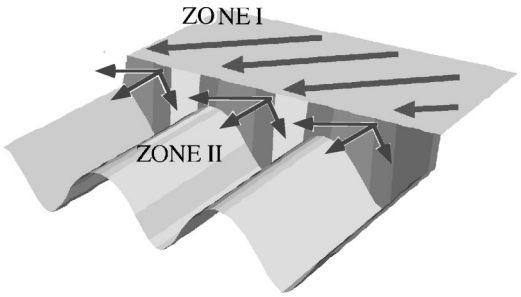

FIG. 1. Scheme of the potential geometry considered. The target-vacuum interface extends over the $x=0$ plane. The potential is already shown in the continuum approximation.

fore will remain close to the initial trajectory. The proper description of this process should take as a starting point the Dirac equation

$$i\hbar\frac{\partial\Psi(\mathbf{r},t)}{\partial t}=[c\boldsymbol{\alpha}\cdot\mathbf{p}+\beta mc^2+V(\mathbf{r})]\Psi(\mathbf{r},t), \tag{1}$$

where we suppose an infinite target in the y,z plane, while of limited size in the x direction

$$V(\mathbf{r})=\begin{cases}0, & x<0,\\ V(x,y,z), & x\geqslant 0.\end{cases} \tag{2}$$

As standard in wave problems, the surface of the target potential (at $x=0$) divides the space into two complementary regions, see Fig. 1. In the $x<0$ half space, the electron propagates in vacuum and the wave function may be expressed in terms of the free Dirac electron eigenstates

$$\Psi_I(\mathbf{r},t)=e^{-i\varepsilon_r(p_0^\mu\cdot x_\mu)/\hbar}u^r(\mathbf{p}), \tag{3}$$

where $p_0^\mu=(E_0,\mathbf{p}_0)$ the initial four-momentum, with $(E_0=\sqrt{c^2|\mathbf{p}_0|^2+m^2c^4})$, $u^r(\mathbf{p})$ with $r=1,2,3,4$ the four possible Dirac free spinors and $\varepsilon^r=+1$ for $r=1,2$ and $\varepsilon^r=-1$ for $r=3,4$. Since the scattering with the target involves mainly nonrelativistic momenta exchange, the reflection at the interface can be neglected. In this case, the particle in the first zone can be described directly as the plane wave (3). The condition of the electron's trajectory nearly parallel to the x axis implies nonrelativistic transversal momentum components, $(p_x)_0\gg(p_y)_0,(p_z)_0$.

In the second zone, the eigenstate of the electron diffracted by the target's potential can be factorized as

$$\Psi_{II}(\mathbf{r},t)=e^{-i\varepsilon_r E_0 t/\hbar}e^{i\varepsilon_r[(p_x)_0x]/\hbar}\psi^r(x,y,z), \tag{4}$$

$\psi^r(x,y,z)$ being a slowly varying spinor

$$|\nabla\psi^r|\ll\frac{(p_x)_0}{\hbar}|\psi^r|. \tag{5}$$

Let us now make explicit the spinor character of the slowly varying envelope. For this we use the free electron base

$$\begin{aligned}\psi^r(x,y,z)&=\int dp_x dp_y dp_z\xi(p_x,p_y,p_z)e^{i\varepsilon_r(p_xx+p_yy+p_zz)/\hbar}\\&\quad\times u^r((p_x)_0+p_x,p_y,p_z)\\&=u^r(\hat{\mathbf{p}})\xi^r(x,y,z),\end{aligned} \tag{6}$$

where we have defined $u^r(\hat{\mathbf{p}})$ as a spinor operator, diagonal in the free particle base.

For simplicity let us assume in the following a particle of positive energy, $r=1$. Therefore, we shall drop the label r writing ψ^1 as

$$\psi(x,y,z)=u(\hat{\mathbf{p}})\xi(x,y,z)=\int dp_x dp_y dp_z\xi(p_x,p_y,p_z)\begin{pmatrix}1\\0\\\dfrac{cp_z}{E+mc^2}\\\dfrac{c[p_x+(p_x)_0+ip_y]}{E+mc^2}\end{pmatrix}e^{i(p_xx+p_yy+p_zz)/\hbar}. \tag{7}$$

Substituting in the Dirac equation for the second spatial zone, we have three scalar equations corresponding to each nonzero component of the spinor. The first equation reads

$$\begin{aligned}&\left\{E_0-\frac{c^2|\hat{\mathbf{p}}|^2}{\hat{E}+mc^2}-V(x,y,z)-mc^2\right\}\xi(x,y,z)\\&\quad=\{E_0-\hat{E}-V(x,y,z)\}\xi(x,y,z)=0,\end{aligned} \tag{8}$$

where $\hat{E}^2=c^2|\hat{\mathbf{p}}|^2+m^2c^4$. The slow-varying envelope approximation applied to the energy operator gives

$$\hat{E}\approx(E_x)_0\left[1+\frac{c^2}{2}\left(\frac{2(p_x)_0\hat{p}_x+\hat{p}_y^2+\hat{p}_z^2}{(E_x)_0^2}\right)+O\left(\frac{c^2\hat{p}_x^2}{(E_x)_0^2}\right)\right], \tag{9}$$

where $(E_x)_0^2=c^2(p_x)_0^2+m^2c^4$ is the initial energy of the electron's longitudinal displacement. Introducing Eq. (9) into Eq. (8) one finally obtains

$$\left\{ E_0 - (E_x)_0 - \frac{c^2(2(p_x)_0\hat{p}_x + \hat{p}_y^2 + (p_z)_0^2)}{2(E_x)_0} - V(y) \right\} \xi(x,y) = 0. \tag{10}$$

It is possible to find *identical* approximated equations for all of the spinor components of the wave function, by using

$$(\hat{E} + mc^2) V(y) \frac{1}{(\hat{E} + mc^2)} \approx V(y) \tag{11}$$

and

$$\frac{(\hat{E} + mc^2)}{c[(p_x)_0 + \hat{p}_x + i\hat{p}_y]} V(y) \frac{c[(p_x)_0 + \hat{p}_x + i\hat{p}_y]}{(\hat{E} + mc^2)} \approx V(y), \tag{12}$$

and taking into account that the crystal potential energy is nonrelativistic, i.e., a quantity of the order $V(x,y,z) \sim O(c^2(\hat{p}_x)^2/(mc^2))$. Naturally, the reduction of the Dirac equation to a simple scalar form is a consequence of the lack of relativistic momentum components in the target's potential.

To compute the form of the eigenstate in the second spatial zone, we just rewrite Eq. (10) in a more familiar form

$$i\hbar \frac{\partial \xi(x,y)}{\partial [x/(v_x)_0]} = \left((E_x)_0 - E_0 + \frac{\hat{p}_y^2 + \hat{p}_z^2}{2(\gamma_x)_0 m} + V(x,y,z) \right) \xi(x,y,z), \tag{13}$$

being $(\gamma_x)_0 = (E_x)_0/(mc^2)$ and $(v_x)_0 = (p_x)_0/[(\gamma_x)_0 m]$. Note that this has the formal appearance of a two-dimensional (2D) time-dependent Schrödinger equation, in which the time variable is replaced by $x/(v_x)_0$. We should point out that this is *not* the eigenstate equation generally used for the problem of channeling, which neglects the longitudinal dynamics and shows up simply as a 2D time-*independent* Schrödinger equation [4,10]. This difference shows that the edge of the target potential has dynamical consequences and introduces a spatial dependence along the longitudinal coordinate.

III. EIGENSTATES OF PLANAR CHANNELING OF ELECTRON IN SILICON (110)

Equation (13) was derived independently of the form of the target potential, as long as it is smooth enough to avoid the exchange of relativistic momenta during the scattering process. The problem of fast particle channeling into crystal structures is particularly well suited for this approach. We will focus the rest of this paper on studying the particular case of the channeling of a relativistic electron, injected almost parallel to the (110) plane.

In fact, the channeling problem allows a further approximation — the so-called continuum approximation [8] — in which the crystal potential is averaged over the channel direction. In case of axial channeling, for instance, the approximation averages the target potential along the crystal axis. For the case of planar channeling, the average should be carried over a crystal symmetry plane. As a result of the averaging, the continuum potential in the crystal bulk becomes independent of the longitudinal coordinate, and its dimensionality is reduced, accordingly, to 2D in the axial case and 1D in the planar case. In our particular case, therefore, the continuum approximation allows us to write the scattering potential in the following form:

$$V(\mathbf{r}) = \begin{cases} 0, & x < 0, \\ V(y), & x \geqslant 0, \end{cases} \tag{14}$$

where y refers to the transversal coordinate perpendicular to the crystal planes.

The continuum potentials are generally computed by averaging Thomas-Fermi [8] or Hartree [11] single-ion potentials, or by means of multiwave calculations in Fourier space. All these forms lead accurately to a transversal energy spectra consistent with the experimentally observed transitions. In any case, we must underline that the continuum approximation is *not* necessary to solve Eq. (13) numerically, since the computational effort required is well below the limit of today's computers. However, since their validity has been examined experimentally [9], there is no reason to think that using directly the single-ion potentials will have important consequences. It seems, therefore, reasonable to use in the present paper the continuum approximation, to take advantage of the reduction of dimensionality, which speeds dramatically the calculation of Eq. (13).

In the present paper, we will use the continuum potential proposed by Avetissian *et al.* [12], in which the interplanar potential is described in terms of the transversal coordinate as

$$V(y) = -V_0 \sum_{n=-\infty}^{\infty} \cosh^{-2}\left(\frac{y - nd_p}{b} \right), \tag{15}$$

where d_p is the distance between symmetry planes [$\simeq 2$ Å for Si (110) planes] and b and V_0 are parameters used to fit the energy spectra to the known experimental data. This potential is known to be less accurate than the model used by Berman *et al.* [9], but presents the considerable theoretical advantage that it admits an analytical diagonalization, which will be used in Sec. V. To minimize errors, we have chosen $b = 0.265$ Å and $V_0 = 19.86$ eV to reproduce accurately the transition energy between the fundamental and the first excited channel states, for an electron energy of 17.48 MeV of Berman's paper. For these parameters, the energy of the second and third excited states is reproduced with an error of $\simeq 0.5$ and $\simeq 0.9$ eV, respectively.

The propagation of the electron in free space, before entering the target, supplies boundary conditions to the wave

function in the second zone of the scattering problem. Therefore, knowing the plane-wave structure of the electron wave in the first zone, Eq. (13) can be integrated only in the target space $x>0$ imposing the continuity condition $\Psi_I(0,y)=\Psi_{II}(0,y)$. To solve Eq. (13) from this boundary condition we use a split operator method, which is a fundamental algorithm frequently used for the time integration of the Schrödinger equation. Basically, this algorithm computes the wave function at any point (x,y), $\xi(x,y)$, from its known value at $(x-\Delta x,y')$, for all y', by using the ''time-evolution'' operator

$$\xi(x,y)=\exp[-iH\Delta x/\hbar(v_x)_0]\xi(x-\Delta x,y), \tag{16}$$

where

$$H=(E_x)_0-E_0+\frac{\hat{p}_y^2}{2(\gamma_x)_0 m}+V(y). \tag{17}$$

The ''evolution'' operator is then (second-order) approximated by its splitted form

$$\exp[-iH\,\delta x/(v_x)_0] \simeq \exp[-iH_1\delta x/\hbar(v_x)_0]\exp[-iH_2\delta x/\hbar(v_x)_0], \tag{18}$$

where H_1 gathers the spatial terms of H and, therefore, is diagonal in the real space, while H_2 encloses the momentum terms of H, being diagonal in the momentum space. The split operator algorithm applies the following sequence of operators:

$$\xi(x,y)=\exp[-iH_1\Delta x/\hbar(v_x)_0]M^{-1} \times\exp[-iH_2\Delta x/\hbar(v_x)_0]M\xi(x-\Delta x,y), \tag{19}$$

where M is a spatial Fourier transform operator.

Figure 2 shows the squared modulus of computed eigenstates for the case of a 17.48 MeV electron injected in the Si crystal almost parallel to the (110) plane, and for three different values of the initial transversal momentum, p_y, labeled by the tilt angle $\theta\simeq cp_y/E_0$ of the initial trajectory to the symmetry plane. The probabilities are depicted over a transversal extension corresponding to three interplanar distances d_p. Channeling shows up as an increase of the probability density at the location of the crystal planes ($y=-d_p$, 0 and d_p), where the transversal potential is minimum. After channeling occurs the behavior of the electron probability with the crystal length x is largely nontrivial, and reflects the important contribution of the longitudinal dynamics induced by the crystal edge where the electron enters the target. As the tilt angle increases, the electron probability in the interplanar spaces is larger, reflecting the fact that part of the wave function is dechanneled. In particular, there are experimental evidences that channeling is negligible for tilt angles above 2 mrad [9]. This case is shown in Fig. 2(c), where practically all the electron probability flows through the channels.

The longitudinal dynamics has an important role in modifying the angular distribution of the electron transmission at different crystal lengths. Figure 3 shows the angular distribution of the transmitted electron probability as it exits the

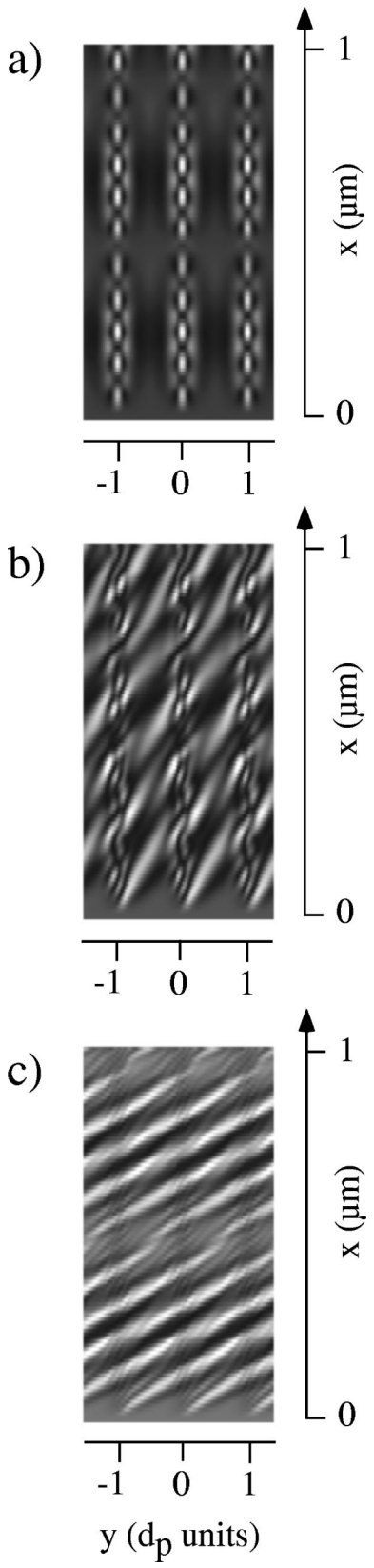

FIG. 2. Electron probability distribution in the crystal bulk, after crossing the target-vacuum interface (at $x=0$). The electron is injected along the Si (110) plane with an initial electron energy of 17.48 MeV, and tilt angles of 0 (a), 1 (b), and 2 mrad (c).

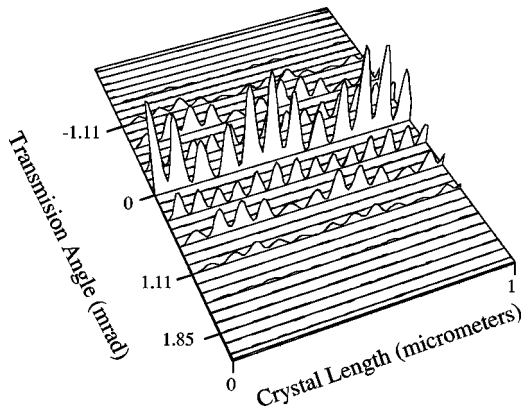

FIG. 3. Angular dependence of the transmission coefficient of an electron injected parallel to the Si (110) plane, perpendicularly to the target surface (tilt angle 0). Since the electron is initially a plane wave, the electron transmitted has a discrete angular spectrum, which corresponds to the diffraction pattern after absorbing a different number of crystal momenta $2\pi/d_p$. The transmission coefficients at a particular angle of detection show modulations with the crystal thickness as a consequence of the longitudinal dynamics induced by the scattering with the target surface.

target of different lengths. It is worth noting the approximate periodic behavior of this quantity with the target length. Figure 4 shows the transmitted probability at four fixed angles as a function of crystal length. A dependence with the target thickness has been observed already for a long time, for instance, in Cu crystals [8,13], and attributed to Bloch-wave absorption effects. To the authors' knowledge, however, the analysis of this point has not been addressed intensively in the experiments.

IV. CHANNELING PROBABILITIES

A more cumbersome method of solution of Eq. (13) consists in finding the complete basis of the transversal dynamics by solving the eigenstate problem

$$\epsilon_n \phi_{\mathbf{K},n}(x,y,z) = \left((E_x)_0 - E_0 + \frac{\hat{p}_y^2 + (p_z)_0^2}{2(\gamma_x)_0 m} + V(y,z) \right) \phi_{\mathbf{K},n}(x,y,z), \tag{20}$$

where n labels the corresponding energy band, and $\mathbf{K}$ the transverse pseudomomentum. Once the elements of the basis are known, the full solution of Eq. (13) may be found as a superposition of these states

$$\xi(x,y,z) = \int d\mathbf{K} \sum_n a_n(\mathbf{K}) \phi_{\mathbf{K},n}(y,z) \exp[-i\epsilon_n x/(v_x)_0]. \tag{21}$$

In general, the computation of the transversal eigenstates requires more computer power than using the method outlined above. Moreover, the expansion (21) is valid only if the target potential $V(x,y,z)$ becomes x independent in the bulk, while the procedure discussed in Sec. III has not this restriction and can be applied, for example, to study the effect of dislocations or to bent crystals [10]. In any case, Eq. (21) is still interesting since the standard definition of a channel state corresponds to any bound eigenstate of the transversal potential $V(y,z)$. The probability of channeling in a given bound-state $\phi_{\mathbf{K},m}(y,z)$ corresponds, therefore, to $|a_m(\mathbf{K})|^2$. The particular value of this channeling probability is determined by the shape of the electron wave function at the target boundary. For a free electron entering the crystal with a transversal momentum k_y, $a_m(\mathbf{K})$ is just the k_y Fourier transform of $\phi_{k_y,m}(y,z)$.

In the case of the model potential (15), it is possible to obtain an analytical approximation to the channeling probabilities in a closed form. For this, we first have to note that the crystal potential is constructed as a superposition of single-cell potentials of the form $V_0 \cosh^{-2}(y/b)$, which allows for an analytical diagonalization. For instance, the solution of Eq. (20) for a single-cell potential gives eigenstates of the form [14]

$$\phi_n(y) = \cosh^{n-s}(y/b)_2 \times F_1(-n, 2s-n+1, s-n+1, [1-\tanh(y/b)]/2,), \tag{22}$$

where $s = [-1+\sqrt{1+8(\gamma_x)_0 m b^2 U_0/\hbar^2}]/2$ and $n = 0,1,\ldots,[s]$ being the largest integer value not greater than s. Since the first argument of the hypergeometric function is an integer, they can be expanded in a finite sum [15]

$${}_2F_1(-n,b,g,z) = \frac{z^{1-g}(1-z)^{g+n-b}}{g(g+1)(g+n-1)} \frac{d^n}{dz^n}[z^{g+n-1}(1-z)^{b-g}]. \tag{23}$$

For the case considered in this paper, the number of possible bound states is $[s]+1=4$, and their respective expressions are

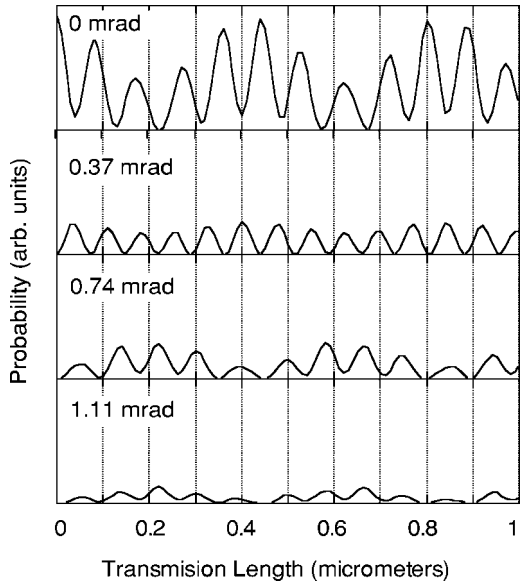

FIG. 4. Transmitted probability at tilt angles 0, 0.37, 0.74, and 1.11 mrad as a function of crystal length.

$$\phi_{n=0}(y)=C_0\cosh^{-s}(y/b), \tag{24}$$

$$\phi_{n=1}(y)=C_1\cosh^{1-s}(y/b)\tanh(y/b), \tag{25}$$

$$\phi_{n=2}(y)=C_2\left(\cosh^{2-s}(y/b)\tanh^2(y/b) - \frac{1}{2(s-1)}\cosh^{-s}(y/b)\right), \tag{26}$$

$$\phi_{n=3}(y)=C_3\left(\cosh^{3-s}(y/b)\tanh^3(y/b) - \frac{3}{2(s-2)}\cosh^{1-s}(y/b)\tanh(y/b)\right), \tag{27}$$

with C_i the correspondent normalization constants that can be found in the Appendix.

Since the channeled states have the lower energy of the transversal spectrum, it is reasonable to approximate them by the first-order tight-binding form

$$\Phi_{K,n}(y)=\frac{1}{N}\sum_{l=0}^{N} e^{ilKd_p}\phi(y-ld_p). \tag{28}$$

Therefore, for an electron initially free with transversal momentum $(k_y)_0$, one finds the probability amplitude for a given channel state as

$$a_{K,n}[(k_y)_0]=\int_{-\infty}^{\infty}\Phi^*_{K,n}(y)e^{i(k_y)_0 y}dy=\delta_{\{(k_y)_0,K+j2\pi/d\}} \times\int_{-\infty}^{\infty}\phi^*_{K,n}(y)e^{i(k_y)_0 y}dy,$$

$$a_{K,n}[(k_y)_0]=\delta_{\{(k_y)_0,K+j2\pi/d\}}a_n(k). \tag{29}$$

Being $a_n(k)=\int_{-\infty}^{\infty}\phi^*_{K,n}(y)e^{i(k_y)_0 y}dy$ the remaining Fourier integral, which can be solved analytically

$$a_{n=0}(k)=2^s bC_0\left(\frac{{}_2F_1\left(\frac{z}{2},s,\frac{z+2}{2},-1\right)}{z}+\text{c.c.}\right), \tag{30}$$

where we have defined the complex parameter z as $z=s+ibk$.

$$a_{n=1}(k)=b2^{s-1}C_1\left[\left(\frac{{}_2F_1\left(\frac{z+1}{2},s,\frac{z+3}{2},-1\right)}{(z+1)}+\text{c.c.}\right) -\left(\frac{{}_2F_1\left(\frac{z-1}{2},s,\frac{z+1}{2},-1\right)}{(z-1)}+\text{c.c.}\right)\right], \tag{31}$$

$$a_{n=2}(k)=b2^{s+1}C_2\left(\frac{{}_2F_1\left(\frac{z-2}{2},s,\frac{z+4}{2},-1\right)}{(z-2)z(z-2)}+\text{c.c.}\right) -\frac{C_2 a_{n=0}(k)}{2C_0(s-1)}, \tag{32}$$

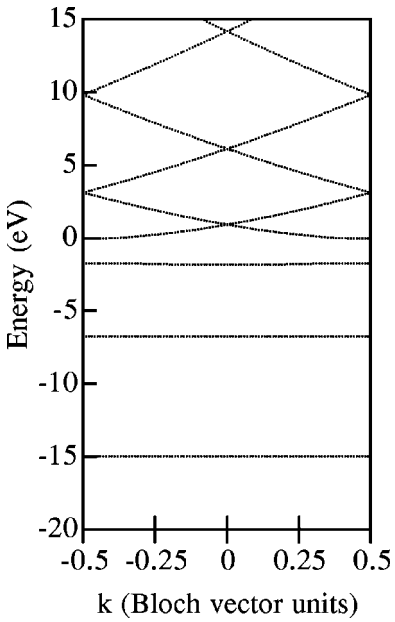

FIG. 5. Energy-band structure of the continuum potential (15).

$$a_{n=3}(k)=3b2^{s+1}iC_3\left(\frac{{}_2F_1\left(\frac{z-3}{2},s,\frac{z+5}{2},-1\right)}{(z-3)(z-1)(z+1)(z+3)}-\text{c.c.}\right) -\frac{3C_3 a_{n=1}(k)}{2C_1(s-2)}. \tag{33}$$

In order to test the accuracy of the tight-binding assumption, we have performed numerically the diagonalization of Eq. (20). Figure 5 shows the energy bands calculated in this case. Since the lowest-order tight-binding approximation used in Eq. (28) leads to flat bands, the inspection of this figure permits us to estimate qualitatively the validity of this assumption. According to this, the three lowest-channel states are well approximated by the tight-binding model, while being less accurate for the fourth. In support of this assertion, Fig. 6 depicts the spectral form of the eigenstates of the first three bands of the transverse spectrum, and compares with the results using the tight-binding assumption. As expected, the tight-binding states reproduce with good accuracy these states.

As discussed in Eq. (29), the spectra shown in Fig. 6 correspond also to the probability of the free electron to be scattered by the target potential into a channeled band. Consistent with the known facts, the probabilities for channeling in any state are reduced to tilt angles below 2 mrad. As one may expect, the total probability of channeling (i.e., the addition of the probabilities over all channel states) is maximum when the electron is injected perpendicularly to the target surface.

Channel population inversion

An alternative possibility for the channeling process is the coherent amplification of high-frequency radiation. In this use, the electron is injected together with a copropagating

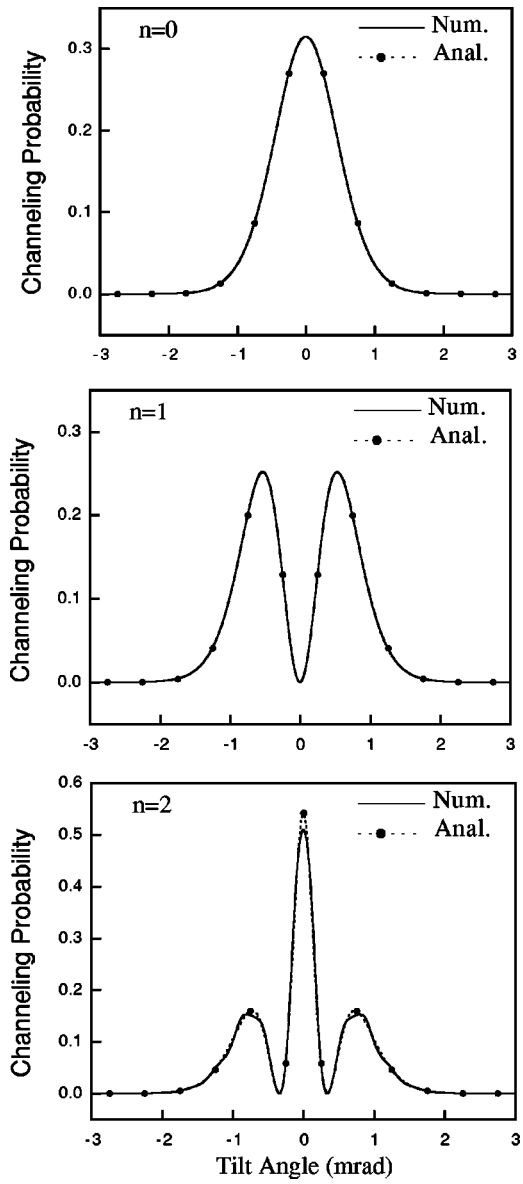

FIG. 6. Spectral distributions of the first three channeled states in Si (100), using the potential (15). Results from the exact numerical diagonalization are shown by solid lines, while analytical results coming from the lowest-order tight-binding approximation are superimposed using a dot-circle line.

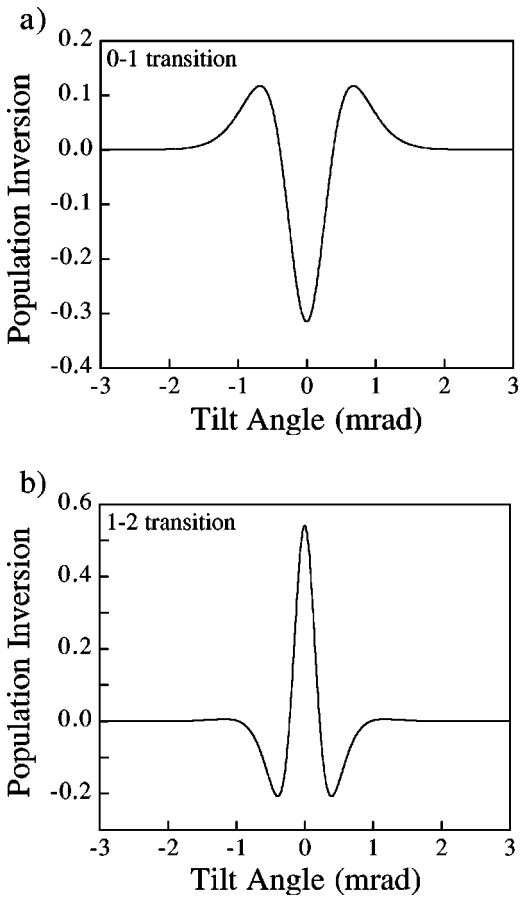

FIG. 7. Population inversion for the two possible dipolar transition between Si (110) channeled states of a 17.48 MeV electron.

electromagnetic wave, whose frequency is nearly resonant to the Doppler-shifted channel transition. In fact, this constitutes a twofold problem: First a mechanism for generating population inversion among the channel states should be proposed and, second, the conditions for maximum gain must be found. This second aspect has already been addressed by Avetissian *et al.* [12], assuming a complete inverted transition. Unfortunately, it is shown that an enormous current density, large enough to produce damage into the crystal, is required to obtain visible amplification gain.

The results plotted in Fig. 6 demonstrate the possibility of controlling channel population by modifying the tilt angle of the initial electron's trajectory. This feature can be directly applied to delimit situations in which a population inversion can be achieved. Figure 7 shows the population inversion on the transitions between channeled states $0-1$ and $1-2$ as generated by the scattering of the electron with the target surface with different tilt angles. As can be clearly seen, the population inversion of the transition between the fundamental and first excited channel states $(0-1)$ can be achieved for electron trajectories tilted about 0.5 mrad, while the optimal situation to obtain inverted population in the $1-2$ transition is when the electron is injected perpendicularly to the surface.

V. CONCLUSIONS

We have presented a theoretical analysis of the channeling process, taking as a starting point a free electron propagating in vacuum, and including the dynamical effects of the scattering of the particle with the target-vacuum interface. As a main result, we demonstrate that the surface scattering induces a rich longitudinal dynamics, in addition to the already well-known transversal motion in the channel. To solve the full — longitudinal and transversal — channeling problem, we have presented a method which does not require the diagonalization of the full Hamiltonian, and that can be also used in the most general case of a channeling potential with longitudinal dependence, as in the case of bent crystals. In particular, we have used this method to analyze the planar channeling of relativistic electrons in the (110) plane of the

Si crystal. We demonstrate that the longitudinal dynamics induced by the surface scattering has a relevant role in the dependence of the transmitted electron's angular distribution with the crystal thickness. According to this, the variation recorded in experiments should be attributed to the surface scattering problem instead to absorption effects. We have also addressed the problem of computing the channeling probabilities of the scattered electron, and given approximated closed analytical expressions of those. As a result of this analysis, we spot the possibility of generating population inversion of a given channel transition for particular tilt angles. However, in this case, the existence of population inversion does not imply lasing [12].

ACKNOWLEDGMENTS

We would like to thank Professor F. H. M. Faisal for enlightening discussions. This work has been supported by the Spanish Dirección General de Enseñanza Superior e Investigación Científica (Grant No. PB98-0268), and the Junta de Castilla y León in collaboration with the European Union, F.S.E. (SA080/02).

APPENDIX

The normalization coefficients of the three bound states of lower energy, Eqs. (24)–(26),

$$\frac{1}{C_0^2}=\frac{b\sqrt{\pi}\Gamma(s)}{\Gamma(s+1/2)}, \tag{A1}$$

$$\frac{1}{C_1^2}=\frac{b}{2}\left(\frac{\sqrt{\pi}\Gamma(s+1)}{2(s-1)\Gamma(s+1/2)}-\frac{\sqrt{\pi}\Gamma(s)}{\Gamma(s+1/2)}+\frac{2(s+1)+4^s(s-1)_2F_1(2s,s+1,s+2,-1)}{2(s^2-1)}\right), \tag{A2}$$

$$\begin{aligned}\frac{1}{C_2^2}=\frac{b}{32}\Bigg(&-\frac{8(s-3)s}{(s-2)(s-3)^2}+\frac{4^s s^3(s^2+s-3)\Gamma(s-2)\Gamma(s-1)}{(s-1)(s+2)\Gamma(2s)}\\&+\frac{4\sqrt{\pi}(s^5-s^4-5s^3-4)\Gamma[s-2]}{(s^2-1)(s+2)\Gamma[s+1/2]}+\frac{4\sqrt{\pi}(5s+4)\Gamma(s+1)}{(s^2-1)(s-1)(s^2-4)\Gamma(s+1/2)}\\&+\frac{4^s\Gamma^2(s+1)[4\Gamma(2s)-\Gamma(2s+1)]}{(s-1)^3(s^2-4)\Gamma(2s)\Gamma(2s+1)}+\frac{2^{2s+3}s_2F_1(2s,s+1,s+2,-1)}{s^2-1}\\&+\frac{2^{2s+1}s_2F_1(2s,s+2,s+3,-1)}{s+2}\Bigg).\end{aligned} \tag{A3}$$

[1] J. Stark and G. Wendt, Ann. Phys. (Leipzig) **38**, 921 (1912); J. Stark, J. Phys. Z **13**, 973 (1912).
[2] M.T. Robinson, Appl. Phys. Lett. **1**, 49 (1962).
[3] P.K. Rol, J.M. Fluit, F.P. Viehböck, and M. De Jong, in *Proceedings of the Fourth International Conference on Ionization Phenomena in Gases*, edited by N.R. Nilsson (North-Holland, Amsterdam, 1960), p. 257.
[4] A review on this may be found in J.C. Kimball and N. Cue, Phys. Rep. **125**, 69 (1985).
[5] Described in M.A. Kumakhov, Phys. Lett. **57A**, 17 (1976).
[6] F.H.M. Faisal and J.Z. Kamiński, Phys. Rev. A **54**, R1769 (1996); **56**, 748 (1997); **58**, R19 (1998).
[7] C.K. Gary, A.S. Fisher, and R.H. Pantell, Phys. Rev. B **42**, 7 (1996).
[8] D.S. Gemmell, Rev. Mod. Phys. **46**, 129 (1974).
[9] B.L. Berman *et al.*, in *Relativistic Channeling*, edited by R.A. Carrigan and J.A. Ellison (Plenum Press, New York, 1986).
[10] A.V. Solov'yov, A. Schäfer, and W. Greiner, Phys. Rev. E **53**, 1129 (1996).
[11] P.A. Doley and P.S. Turner, Acta Crystallogr., Sect. A: Cryst. Phys., Diffr., Theor. Gen. Crystallogr. **26**, 390 (1968).
[12] H.K. Avetissian, K.Z. Hatsagortsian, G.F. Mkrtchian, and Kh.V. Sedrakian, Phys. Rev. A **56**, 4121 (1997).
[13] F. Fujimoto *et al.*, Radiat. Eff. **12**, 153 (1972).
[14] L.D. Landau and E.M. Lifshitz, *Quantum Mechanics: Non-relativistic Theory*, 3rd ed. (Pergamon, Oxford, 1977).
[15] The properties of the hypergeometric functions can be found in the "e" mathematical appendix of Ref. [14], and also in M. Abramowitz and I.A. Stegun, *Handbook of Mathematical Functions*, 10th ed. (Dover, New York, 1972), Chap. 15.